Research on Amplitude and Polarization Characteristics of Array Ground Penetrating Radar in Three-dimensional Space

Yi Chen[1], Fan Cui[1], and Yongqi Zhang[1]

[1]China University of Mining and Technology (Beijing)

November 24, 2022

Abstract

A conventional single dipole antenna will make the antenna power gain effect poor,and the energy of the effective excitation signal and scattering signal reflected from underground detection target(such as interface, metal target) is also weak, problems such as shallow detection depth, low target resolution, and weak signal anti-interference ability will occur. Array radar uses a multi-emission and multi-acceptance method to detect underground targets-multiple transmitting antennas simultaneously excite electromagnetic pulse signals of the same center frequency, and the electromagnetic energy is superimposed on each other. When electromagnetic waves encounter the target, obvious polarization can occur.In this paper,the complex frequency shift (CFS) perfectly matched layer (PML) is used as the absorbing boundary condition, which can effectively absorb outwardly propagating electromagnetic waves to simulate an infinite three-dimensional space.Use VTK to visualize the propagation wave field of electromagnetic waves in the three-dimensional model space, track the full waveform of electromagnetic waves in the three-dimensional model space, and analyze the polarization characteristics of electromagnetic waves under different observation methods.In order to improve the low efficiency of FDTD numerical calculation, GPU is used in the simulation to accelerate the calculation of the iterative solution of FDTD. By comparing the simulation data of the array radar and the forward data of the single-shot single-receive ground penetrating radar, it is concluded that the array radar observation method has advantages in improving the echo signal, enhancing the polarization characteristics, and improving the target resolution and accuracy.

Chen Yi(Orcid ID:0000-0001-8777-2828)

Cui Fan(Orcid ID:0000-0001-5102-8394)

Research on Amplitude and Polarization Characteristics of Array Ground Penetrating Radar in Three-dimensional Space

Chen Yi[1,2,3],Cui Fan1[1,2,3],Zhang Yongqi[1,2]

1School of Geosciences and Surveying Engineering, China University of Mining and Technology (Beijing), Beijing, China

2State Key Laboratory of Coal Resources and Safe Mining, China University of Mining and Technology (Beijing), Beijing, China

3Beijing Key Laboratory for Precise Mining of Intergrown Energy and Resources, Beijing, China.

Corresponding author:Chen Yi(cy18729242764@163.com)

Abstract:

A conventional single dipole antenna will make the antenna power gain effect poor,and the energy of the effective excitation signal and scattering signal reflected from underground detection target(such as interface, metal target) is also weak, problems such as shallow detection depth, low target resolution, and weak signal anti-interference ability will occur. Array radar uses a multi-emission and multi-acceptance method to detect underground targets—multiple transmitting antennas simultaneously excite electromagnetic pulse signals of the same center frequency, and the electromagnetic energy is superimposed on each other. When electromagnetic waves encounter the target, obvious polarization can occur.In this paper,the complex frequency shift (CFS) perfectly matched layer (PML) is used as the absorbing boundary condition, which can effectively absorb outwardly propagating electromagnetic waves to simulate an infinite three-dimensional space.Use VTK to visualize the propagation wave field of electromagnetic waves in the three-dimensional model space, track the full waveform of electromagnetic waves in the three-dimensional model space, and analyze the polarization characteristics of electromagnetic waves under different observation methods.In order to improve the low efficiency of FDTD numerical calculation, GPU is used in the simulation to accelerate the calculation of the iterative solution of FDTD. By comparing the simulation data of the array radar and the forward data of the single-shot single-receive ground penetrating radar, it is concluded that the array radar observation method has advantages in improving the echo signal, enhancing the polarization characteristics, and improving the target resolution and accuracy.

Keywords: array radar, finite difference time domain (FDTD), VTK, complex frequency shift perfect matching layer (CFS-PML), GPU.

Introduction：

In recent years, ground penetrating radar technology has been widely used in underground engineering detection due to its high precision,convenience, efficiency, flexibility and non-destructiveness[1].With the increasing accuracy of engineering quality requirements, more and more GPR (Ground Penetrating Radar) technologies are used in the detection of small structures.At present, the commonly used ground penetrating radar detection technology is reflection detection, which mainly involves profile ground penetrating radar detection technology , Array radar detection technology[2], wide-angle ground penetrating radar detection technology, etc. Geophysical prospecting needs to obtain high-efficiency and high-quality detection data but the efficiency of the profile method is low and the wide-angle method is mainly used to obtain the speed of underground radar waves. The array radar can not only improve the detection efficiency and signal-to-noise ratio, and realize the underground Multiple coverage of data can also display the visible cross-sectional position of the underground target object, which helps to identify the underground structure.

Ground-penetrating radar (GPR) numerical simulation is not only an effective means to study the propagation law of electromagnetic waves in the complex medium of shallow underground, but also an important basis for research on reverse time migration and full waveform inversion[3] , GPR electromagnetic waves in underground structures Numerical simulation of propagation helps to better explain the real GPR profile[4] .Many numerical simulation methods for ground penetrating radar have been developed at home and abroad, and they are generally divided into two categories: geometric ray method (ray tracing method)[5][6](Cai and McMechan,1995; Huang,etc,2011)and wave equation method.Wave equation method includes finite difference time domain (FDTD)[7][8][9], finite element time domain (FETD)[10][11], pseudospectral time domain (PSTD)[12] and Fourier method[13] etc.Compared with the geometric ray method, the electromagnetic wave field calculated by the wave equation method not only contains the kinematic information of electromagnetic wave propagation, but also contains a wealth of wave information, which can provide more evidence for the study of electromagnetic wave propagation mechanism and the interpretation of complex structures.The finite difference time domain (FDTD) method[14][15][16] proposed by KSYee in 1966 is a method to differentiate Maxwell’s equations and calculate the electric field and magnetic field in space under certain conditions. This method has the advantages of simple principle and convenient program implementation. Therefore, this article uses the FDTD method to simulate the electromagnetic wave of the array radar.

Secondly, the improvement of ground penetrating radar performance and functions has always been the goal pursued by the radar engineering community.For ground penetrating radar, it is not only necessary to clarify where the target is, but also to answer what kind of target it is. This requires the ground penetrating radar to be able to capture the target's size, shape, attitude and other parameter information.Due to the vector nature of electromagnetic waves, polarization characteristics can solve the problem of target characteristic signals and enrich the capture of target information.Therefore, as early as 1946, G. Sinclair of the Ohio State University Antenna Laboratory in the United States proposed to use the "polarized scattering matrix" to characterize the polarized scattering characteristics of radar targets[17],marking the beginning of radar polarization research.In 1970, J.R Huynen explained the internal connection between the polarization scattering matrix elements and the target structure properties[18], point out the possibility of using polarization information for target classification and recognition.In 1986, Guili published a long review on polarization characteristics research[19], marking that the development of radar polarization research is basically becoming mature.After that, Zeng Zhaofa and others from Jilin University conducted an analysis of the polarization field characteristics of the array ground penetrating radar signal[20],compared the polarization characteristics and signal stability of the area array radar and the conventional single-shot single-receive radar, and obtained the area array radar in the recognition The polarization characteristics of the target body are better, and the target signal is more stable.

Finally, a three-dimensional model is established to scan the underground target with a multi-send and multi-receive array antenna group; and the GPU[21][22[23] increases the computing speed to greatly improve the cumbersome and long-time FDTD operations. The polarization characteristic field of electromagnetic waves is tracked on any z-plane, and the polarization characteristics and amplitude characteristics of conventional single-shot single-receive radar and array radar are compared.

Method and principle:

1 Principle of 3D FDTD method:

This paper uses the finite difference time domain method to simulate the motion law of electromagnetic waves in three-dimensional space.Considering a passive region in space whose medium parameters do not change with time, Maxwell's equations evolve into:

$$\frac{\partial H}{\partial \mathrm{t}} = -\frac{1}{\mu}\nabla \times E - \frac{\rho}{\mu}H \qquad (1)$$

$$\frac{\partial E}{\partial \mathrm{t}} = -\frac{1}{\varepsilon}\nabla \times H - \frac{\sigma}{\varepsilon}E \qquad (2)$$

6 coupled partial differential equations can be obtained in three-dimensional space:

$$\begin{cases} \dfrac{\partial H_x}{\partial t} = \dfrac{1}{\mu}\left(\dfrac{\partial E_y}{\partial z} - \dfrac{\partial E_z}{\partial y} - \rho H_x\right) & (3) \\ \dfrac{\partial H_y}{\partial t} = \dfrac{1}{\mu}\left(\dfrac{\partial E_z}{\partial x} - \dfrac{\partial E_x}{\partial z} - \rho H_y\right) & (4) \\ \dfrac{\partial H_z}{\partial t} = \dfrac{1}{\mu}\left(\dfrac{\partial E_x}{\partial y} - \dfrac{\partial E_y}{\partial x} - \rho H_z\right) & (5) \\ \dfrac{\partial E_y}{\partial t} = \dfrac{1}{\varepsilon}\left(\dfrac{\partial H_x}{\partial z} - \dfrac{\partial H_z}{\partial x} - \sigma E_y\right) & (6) \\ \dfrac{\partial E_z}{\partial t} = \dfrac{1}{\varepsilon}\left(\dfrac{\partial H_y}{\partial x} - \dfrac{\partial H_x}{\partial y} - \sigma E_z\right) & (7) \\ \dfrac{\partial E_x}{\partial t} = \dfrac{1}{\varepsilon}\left(\dfrac{\partial H_z}{\partial y} - \dfrac{\partial H_y}{\partial z} - \sigma E_x\right) & (8) \end{cases}$$

Where E is the electric field strength, H is the magnetic field strength, ε is the dielectric constant, σ is the dielectric conductivity, μ is the magnetic permeability, and ρ is the magnetic resistivity for calculating the magnetic loss. Perform Yee difference solution to 6 coupled partial differential equations, and establish a difference grid in space. The grid nodes correspond to a set of corresponding integer labels one to one.

$$(i, j, k) = (i\Delta x, j\Delta y, k\Delta z) \qquad (9)$$

The value of any function $F^{n}(x,y,z)$ at this point at time $\mathrm{n}\Delta t$ can be expressed as

$$F^{n}(i,j,k)=F(i\Delta x, j\Delta y, k\Delta z) \qquad (10)$$

Where $\Delta \mathrm{x}, \Delta y, \Delta z$ are the spatial steps of the rectangular grid along the x, y, and z directions respectively, and Δt is the time step. Yee uses the central difference to replace the differential coordinates of time and space, which has second-order accuracy:

$$\frac{\partial F(i,j,k)}{\partial \mathrm{x}}=\frac{F^{n}(i+\frac{1}{2},j,k)+F^{n}(i-\frac{1}{2},j,k)}{\Delta x}+O(\Delta x^{2}) \quad (11)$$

$$\frac{\partial F(i,j,k)}{\partial \mathrm{t}}=\frac{F^{n+\frac{1}{2}}(i,j,k)+F^{n-\frac{1}{2}}(i,j,k)}{\Delta x}+O(\Delta t^{2}) \qquad (12)$$

In the time domain, the electric field and magnetic field are calculated alternately and iteratively with a difference of half a step. Turn the six coupled partial differential equations into difference equations: at time n:

$$\frac{\partial H_{x}^{n}(i,j+\frac{1}{2},k+\frac{1}{2})}{\partial t}=\frac{H^{n+\frac{1}{2}}(i,j+\frac{1}{2},k+\frac{1}{2})-H^{n-\frac{1}{2}}(i,j+\frac{1}{2},k+\frac{1}{2})}{\Delta t}$$

$$H_{x}=\frac{H^{n+\frac{1}{2}}(i,j+\frac{1}{2},k+\frac{1}{2})+H^{n-\frac{1}{2}}(i,j+\frac{1}{2},k+\frac{1}{2})}{2}$$

$$\frac{\partial E_{y}}{\partial \mathrm{z}}=\frac{E_{y}^{n}(i,j+\frac{1}{2},k+\frac{1}{2})-E_{y}^{n}(i,j+\frac{1}{2},k)}{\Delta z}$$

$$\frac{\partial E_{z}}{\partial y}=\frac{E_{z}^{n}(i,j,k+\frac{1}{2})-E_{z}^{n}(i,j+1,k+\frac{1}{2})}{\Delta y} \qquad (13)$$

Substituting (13) into the partial differential equation (3) and simplifying to obtain the recurrence equation of the magnetic field x component:

$$H_x^{n+\frac{1}{2}}(i, j+\frac{1}{2}, k+\frac{1}{2}) = \frac{1-\dfrac{\rho(i, j+\frac{1}{2}, k+\frac{1}{2})\Delta t}{2\mu(i, j+\frac{1}{2}, k+\frac{1}{2})}}{1+\dfrac{\rho(i, j+\frac{1}{2}, k+\frac{1}{2})\Delta t}{2\mu(i, j+\frac{1}{2}, k+\frac{1}{2})}} H_x^{n-\frac{1}{2}}(i, j+\frac{1}{2}, k+\frac{1}{2}) +$$

$$\frac{\Delta t}{\mu(i, j+\frac{1}{2}, k+\frac{1}{2})} \cdot \frac{1}{1+\{\rho(i, j+\frac{1}{2}, k+\frac{1}{2})\Delta t / [2\mu(i, j+\frac{1}{2}, k+\frac{1}{2})]\}}$$

$$\times \left\{ \frac{E_y^n(i, j+\frac{1}{2}, k+\frac{1}{2}) - E_y^n(i, j+\frac{1}{2}, k)}{\Delta z} + \frac{E_z^n(i, j, k+\frac{1}{2}) - E_z^n(i, j+1, k+\frac{1}{2})}{\Delta y} \right\} \qquad (14)$$

In the same way, the z component and y component of the magnetic field can be obtained.

When solving, the electric field is faster than the magnetic field by 1/2 time step:

$$\frac{\partial E_x}{\partial t} = \frac{E_x^{n+1}(i+\frac{1}{2}, j, k) - E_x^n(i+\frac{1}{2}, j, k)}{\Delta t / 2}$$

$$E_x = \frac{E_x^{n+1}(i+\frac{1}{2}, j, k) + E_x^n(i+\frac{1}{2}, j, k)}{2}$$

$$\frac{\partial H_z}{\partial y} = \frac{H_z^{n+1/2}(i+\frac{1}{2}, j+\frac{1}{2}, k) - H_z^{n+1/2}(i+\frac{1}{2}, j-\frac{1}{2}, k)}{\Delta y}$$

$$\frac{\partial H_y}{\partial z} = \frac{H_z^{n+1/2}(i+\frac{1}{2}, j, k+\frac{1}{2}) - H_z^{n+1/2}(i+\frac{1}{2}, j, k-\frac{1}{2})}{\Delta y} \qquad (15)$$

Substituting equation (15) into the

$$E_x^{n+1}(i+\frac{1}{2},j,k)=\frac{1-\dfrac{\sigma(i+\frac{1}{2},j,k)\Delta t}{2\varepsilon(i+\frac{1}{2},j,k)}}{1+\dfrac{\sigma(i+\frac{1}{2},j,k)\Delta t}{2\varepsilon(i+\frac{1}{2},j,k)}}\cdot E_x^{n}(i+\frac{1}{2},j,k)+$$

$$\frac{\Delta t}{\varepsilon(i+\frac{1}{2},j,k)}\cdot\frac{1}{1+\{\sigma(i+\frac{1}{2},j,k)\Delta t/[2\varepsilon(i+\frac{1}{2},j,k)]\}}$$

$$\times\left\{\frac{H_z^{n+1/2}(i+\frac{1}{2},j+\frac{1}{2},k)-H_z^{n+1/2}(i+\frac{1}{2},j-\frac{1}{2},k)}{\Delta y}+\frac{H_y^{n+1/2}(i+\frac{1}{2},j,k-\frac{1}{2})-H_y^{n+1/2}(i+\frac{1}{2},j,k+\frac{1}{2})}{\Delta z}\right\} \tag{16}$$

In the same way, the recurrence equations of the y and z components of the electric field can be obtained.

2 First-order complex frequency shift (CFS-PML) perfectly matched layer absorption boundary conditions

The wave equation is changed in the complex coordinate in the PML layer. Taking the x direction as an example, the transformation relationship of the frequency domain coordinate in PML is:

$$\tilde{x}(x)=x-\frac{i}{\omega}\int_0^x d_x(s)ds \tag{17}$$

The partial derivative of x is:

$$\partial\tilde{x}=\frac{i\omega}{i\omega+d_x}\partial x=\frac{1}{s_x}\partial x \tag{18}$$

Where: s_x is the complex stretch function; x is the original coordinate; $\tilde{x}$ is the coordinate after transformation; . ω is the circular frequency, d_x is the attenuation coefficient.

The general form of the complex frequency shift stretching function obtained from equation

(19) is:

$$s_x = K_x + \frac{d_x}{\alpha_x + i\omega} \qquad (20)$$

Use $\bar{s}_x(t)$ to represent the inverse Fourier transform of $\frac{1}{s_x}$ to convert frequency domain coordinates into time domain coordinates.

$$\tilde{\partial}_x = \bar{s}_x(t) * \partial_x \qquad (21)$$

Perform inverse Fourier transform on equation (20)and get:

$$\bar{s}_x(t) = \frac{\delta(t)}{K_x} - \frac{d_x}{K_x^2} H(t) e^{-(d_x/K_x+\alpha_x)}$$

Where $\delta(t)$ is the impulse function; $H(t)$ is the unit step function.

Let $$\zeta_x(t) = -\frac{d_x}{K_x^2} H(t) e^{-(d_x/K_x+\alpha_x)t}$$

Then, $$\tilde{\partial}_x = \frac{1}{K_x}\partial_x + \zeta_x(x) * \partial_x \qquad (22)$$

The convolution at discrete time $n\Delta t$ is:

$$\psi_x^{n\Delta t} = (\zeta_x * \partial_x)^{n\Delta t} = \int_0^{n\Delta t} (\partial_x)^{n\Delta t} \zeta_x(\tau) d\tau = \sum_{m=0}^{n-1} \int_{m\Delta t}^{(m+1)\Delta t} (\partial_x)^{(n\Delta t-\tau)} \zeta_x(\tau) d\tau \qquad (23)$$

When the electric and magnetic fields of electromagnetic waves are calculated using alternating grids, there are:

$$\psi_x^{n\Delta t} = \sum_{m=0}^{n-1} (\partial_x)^{((n-(m+1/2))\Delta t)} \int_{m\Delta t}^{(m+1)\Delta t} \zeta_x(\tau) d\tau = \sum_{m=0}^{n-1} Z_x(m) (\partial_x)^{((n-(m+1/2))\Delta t)} \qquad (24)$$

Where:

$$Z_x(m)=\int_{m\Delta t}^{(m+1)\Delta t}\zeta_x(\tau)d\tau=-\frac{d_x}{K_x^2}\int_{m\Delta t}^{(m+1)\Delta t}e^{-(dx/Kx+\alpha x)\tau}d\tau=a_x e^{-(dx/Kx+\alpha x)m\Delta t}$$

and $$a_x=\frac{d_x}{K_x(d_x+K_x\alpha_x)}(b_x-1);b_x=e^{-(dx/Kx+\alpha x)\Delta t}$$

Equation (24) can be simplified as:

$$\psi_x^{n\Delta t}=b_x\psi_x^{(n-1)\Delta t}+a_x(\partial_x)^{(n-1/2)\Delta t} \qquad (25)$$

Perform normal iterative calculations in the model area, and use formula (22) to perform coordinate transformation calculations in PML:

$$\partial\bar{x}=\frac{1}{K_x}\partial_x+\psi_x \qquad (26)$$

Among them, ψ_x can be obtained by recursive formula (25). Carry out coordinate transformation on formula (25) and formula (26) so that the recurrence formula can be calculated alternately in time:

$$\partial_x^{n-1/2}=\frac{1}{K_x}\partial_x^{n-1/2}+\psi_x^{n-1/2}=\frac{1}{K_x}\partial_x^{n-1/2}+\frac{\psi_x^n+\psi_x^{n-1}}{2} \qquad (27)$$

Substituting formula (25) into formula (27) can get:

$$\partial_x^{n-1/2}=\frac{1}{K_x}\partial_x^{n-1/2}+\frac{(b_x+1)\psi_x^{n-1}+a_x(\partial_x)^{n-1/2}}{2} \qquad (28)$$

In the same way, the PML recursive convolution equation of complex frequency shift in y and z directions can be obtained. It is very effective to use the first-order complex frequency shift perfect matching layer (CFS-PML) as the absorbing boundary condition, as shown in Figure 1-a: The electromagnetic wave enters the perfect matching layer without reflection at the boundary and is attenuated.When the conventional perfectly matched layer is used as the absorption boundary condition, the electromagnetic wave will reflect at the boundary and return to the study area, as shown in Figure 1-b.

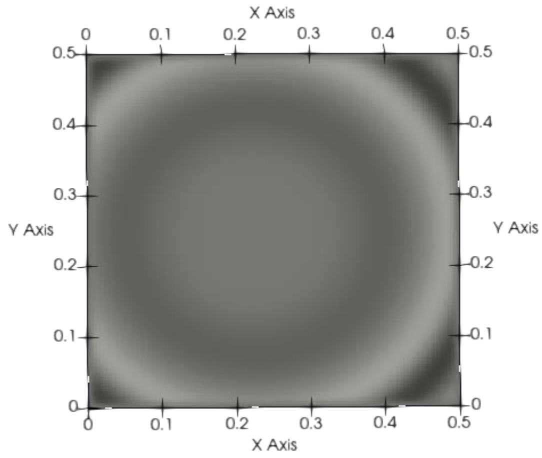

Figure.1-a CFS - PML absorption boundary condition

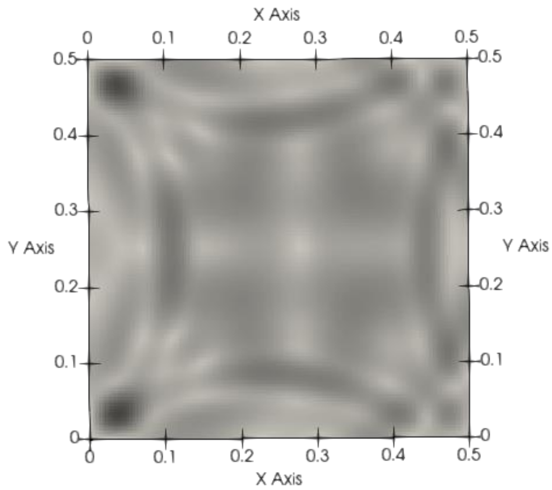

Figure 1-b PML absorption boundary condition

3. Comparison of three-dimensional full wavefield numerical simulation of array radar and single-shot single-receive radar data

3.1 Model description:

Set the size of the model area in the x, y, and z directions to 0.5m.The upper part is air medium with a thickness of 0.1m, and the lower part is a double-layer uniform half space.The first layer is filled with concrete with a thickness of 0.15m. The dielectric constant is 6.0, the conductivity is 0.001S/m, the relative permeability is 1.0, and the magnetic loss is 0Ω/m.A metal sphere with a sphere center of 0.25m×0.25m×0.125m and a radius of 0.05m is buried in the second layer of soil medium.As shown in the figure, an 8×8 array radar is arranged on the concrete surface. The transmitting antenna and receiving antenna of the array radar are arranged in a straight line along the y axis. The spatial position of the first transmitting antenna is 0.035m×0.035m×0.40m,the spatial position of the first receiving antenna is 0.085m×0.035m×0.40m, and the distance between each transmitting antenna is 0.05m. The distance is 0.05m, and the transceiver distance is 0.05m. The 8 transmitting antennas use Hertzian dipoles polarized in the z direction as the excitation source, which uses a Ricker wavelet waveform with a dominant frequency of 900 MHz and a maximum amplitude scaling of 1 ampere.Divide Yee grids in the x, y, and z directions. The spatial step of each grid is 0.004m.The transmitting antenna and the receiving antenna are stepped along the x-axis at the same time. Each step is 0.004m, and 97 channels of data are scanned. Time window given 9ns.The first-order complex frequency shift perfectly matched layer (CFS-PML) is used as the absorbing boundary condition, and the thickness of the fully matched layer on the six sides of the model is 6 spatial steps.The medium parameters of the single-shot single-receive model are the same as those of the array radar, and the spatial position relationship of the model is the same. The excitation point and the receiving point are located at 0.25m×0.25m×0.40m, 0.085m×0.250m×0.40m, and the other parameters are consistent with the array Radar model.The spatial position relationship of the model is shown in Figure 2-a. It took 17 minutes and 32 seconds to run the model under Intel(R) Core(TM) i5-9300H @2.4GHz CPU, and it took 8 minutes and 52 seconds to add the GTX 1650 GPU for auxiliary calculations. Use GPU assisted FDTD loop iteration, the solution saves 8 minutes and 40 seconds.

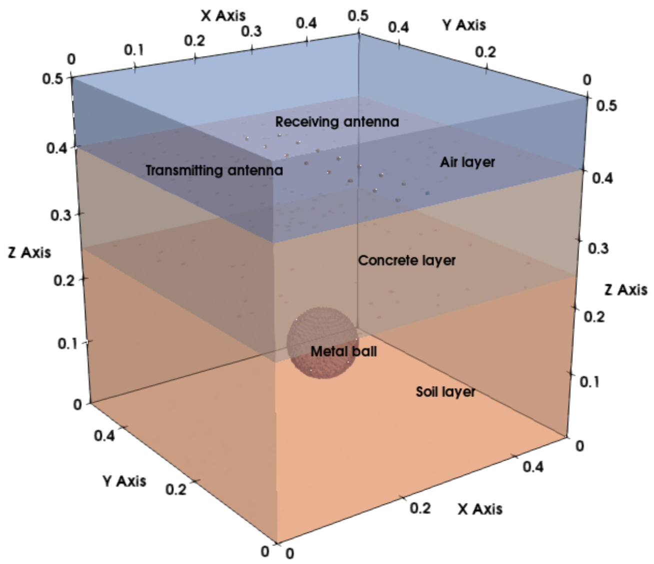

Figure 2-a Three-dimensional model structure diagram

3.2 Comparison and analysis of amplitude characteristics:

The ray path of electromagnetic wave propagation is shown in Figure 2-b,eight transmitting antennas simultaneously emit high-frequency pulsed electromagnetic waves,the electromagnetic waves emitted by each transmitting antenna can be received by each receiving antennas after interfering with each other in space.Multi-point coverage can be achieved when reflection occurs in the underground stratum.

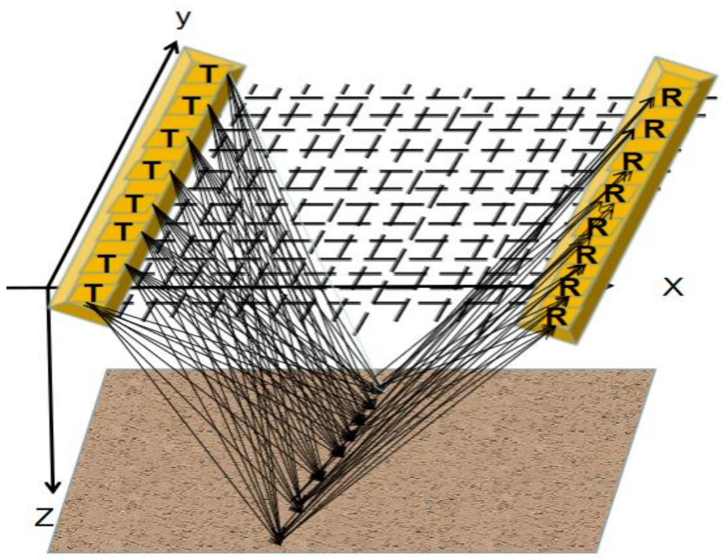

Figure 2-b Electromagnetic wave propagation ray path diagram

According to the principle of interference and superposition of electromagnetic waves: the radiated electromagnetic field generated by the current distribution J in a uniform medium can be expressed as:

$$E = -j\omega A - j\frac{1}{\omega\mu\varepsilon}\nabla(\nabla \cdot A) \qquad (29)$$

$$H = \frac{1}{\mu}\nabla \times A \qquad (30)$$

In the formula, A is called the magnetic vector potential, which satisfies the following Helmholtz equation:

$$\nabla^2 A + k^2 A = -\mu J \qquad (31)$$

When the current density J is distributed along the z-direction line as $zJ_z(z^{'})$ and the length of the distribution line is L, then at the far-field observation point P(x,y,z), the solution of the Helmholtz equation is:

$$A = z\frac{\mu}{4\pi}\int_L \frac{J_z(z^{'})e^{-jkR}}{R}dz^{'} \qquad (32)$$

When multiple dipole antennas are used for radiation, the current can be discretized into the sum of N small parts in total:

$$L = \sum_{n=1}^{N} dl_n \qquad (33)$$

Use $z_n^{'}$ to represent the center coordinates of a small part dl_n of each dipole strip,if dl_n is small enough, the current density of each dipole antenna is uniform and constant in each small part,It can be expressed as $J(z_1^{'})$, $J(z_2^{'})$, $J(z_3^{'})$,..., $J(z_N^{'})$. The formula (32) can be expressed as:

$$A = \sum_{n=1}^{N} A_n = z\sum_{n=1}^{N} A_{zn} = z\frac{\mu}{4\pi}\sum_{n=1}^{N}\frac{J(z_n^{'})dl_n e^{-jkR_n}}{R_n} \qquad (34)$$

In the formula, $J(z_n^{'})dl_n$ represents the total current on a dipole, which is:

$$I_n = J(z_n^{'})dl_n \qquad n = 1,2,3...N \qquad (35)$$

Substituting formula (35) into formula (34) has:

$$A = \sum_{n=1}^{N} A_n = z\frac{\mu}{4\pi}\sum_{n=1}^{N}\frac{I_n e^{-j\omega R_n}}{R_n} \qquad (36)$$

It can be seen from equation (36) that the total radiation field vector potential in space can be expressed as the superposition of N radiation field magnetic vector potentials. Therefore, the E and H of the total radiation electromagnetic field are also formed by the superposition of N parts, namely:

$$E = \sum_{n=1}^{N} E_n$$
$$H = \sum_{n=1}^{N} H_n$$

Simultaneously move the transmitting antenna and the receiving antenna array along the x-axis, scanning 97 channels of data, and extracting the first Ey component field data of the first receiving antenna of the 8×8 array radar as shown in Figure 3.Simultaneously move the transmitting antenna and the receiving antenna array along with the x-axis direction, scanning 97 channels of data, and extracting the first Ey component field data of the first receiving antenna of the 8×8 array, as shown in Figure 3.The single-emitting single-receiving radar moves the transmitting antenna and the receiving antenna along the same path, and also scans 97 channels of data to obtain the first Ey component field data as shown in Figure 4.According to the principle of electromagnetic interference and superposition,Since the array radar uses multiple transmitting antennas to transmit high-frequency pulse electromagnetic waves at the same time, the electromagnetic wave energy emitted by each antenna is superimposed on each other, resulting in a significant increase in the amplitude value.The 8×8 array radar scan data increases the reflected echo energy from the target body compared with single transmission and single reception, and more clearly shows the reflection from the ground and the metal ball.

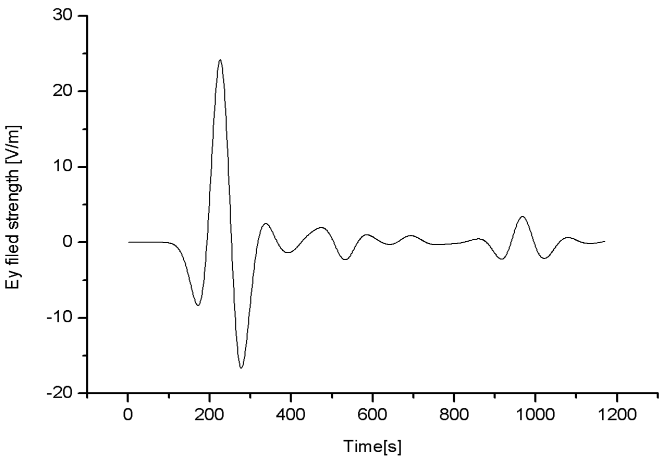

Figure 3 The waveform time history of rec1-Ey component field of 8×8 array radar

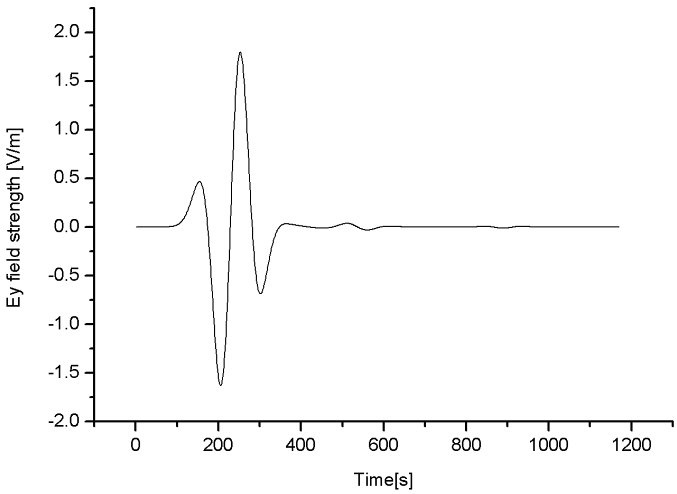

Figure.4 Waveform history of Ey component field of single-dispatch and single-receiver radar

Decompose the incident coefficient and reflection coefficient terms of the target radar in the cross section:

$$rc(\theta_t, \theta_r) = \xi(\theta_t)\xi(\theta_r) \qquad (37)$$

Where θ_t is the incident direction angle and θ_r is the reflection direction angle,due to the single-shot single-receiving radar has a small offset,therefore, $\theta_t \approx \theta_r, \xi(\theta_t) \approx \xi(\theta_r)$ .The reflection coefficient of the receiving antenna observing the target in the θ_r direction is:

$$T_{\text{single}}(\theta_r) = \int_V \xi_x(\theta_r)\xi_x(\theta_r)dx = \int_V \xi_x{}^2(\theta_r)dx \qquad (38)$$

Where T_{single} is the reflection coefficient under the single-shot single-receive radar observation mode, V is the target body and x is a certain point on the target body.When the antenna frequency and transmission waveform of the multi-transmit and multi-receive array radar are the same, the transmitting array signal will be superimposed in space and form a plane wave. Then the reflection coefficient of the receiving antenna in the θ_r direction is:

$$T_{\text{mulit}}(\theta_r) = \int_V \xi_x(\theta_r)\sum_{m=1}^{n} \xi_x(\theta_t)dx \qquad (39)$$

When the antenna center frequency is the same as the transmit waveform, the transmit array signals are superimposed in space to form a plane beam.Then the reflection coefficient of the receiving antenna observing the target in the θ_r direction is:

$$T_{\text{mulit}}(\theta_r) = \int_V [\xi_x(\theta_r)\int_{\theta_1}^{\theta_2}(\xi_x\theta_r)]dx \qquad (40)$$

Where T_{mulit} is the reflection coefficient under the multi-transmit and multi-receive observation mode, n is the total number of transmitting antennas. It can be seen that the size of the reflection coefficient has a linear relationship with the number of transmitting antennas. When there are multiple transmitting antennas,the reflection coefficient will be increased to enhance the echo signal of the target body.Combine the 97-channel scan data, extract the first receiving antenna data, and separate the 97-channel scan Ey component waveform to obtain a vertical cross-sectional profile along the depth z direction. According to equation (30), in the single-shot single-receiving radar observation mode, the electromagnetic wave attenuates rapidly at the first layer of medium, and the reflected electromagnetic fluctuation of the metal ball target is not obvious. Figure 5 shows the Ey component waveform profile of 97 channels of single-transmit and single-receive radar.The Ey component waveform profile of 8×8 array radar data is shown in Figure 6.Because multiple transmitting antennas of the array radar simultaneously excite electromagnetic waves of the same center frequency during observation, the electromagnetic energy is superimposed on each other, and at the same depth, the amplitude value will increase by about 10 times.Electromagnetic waves occur in the lower stratum and the position of the metal ball Obvious wave reflection phenomenon.

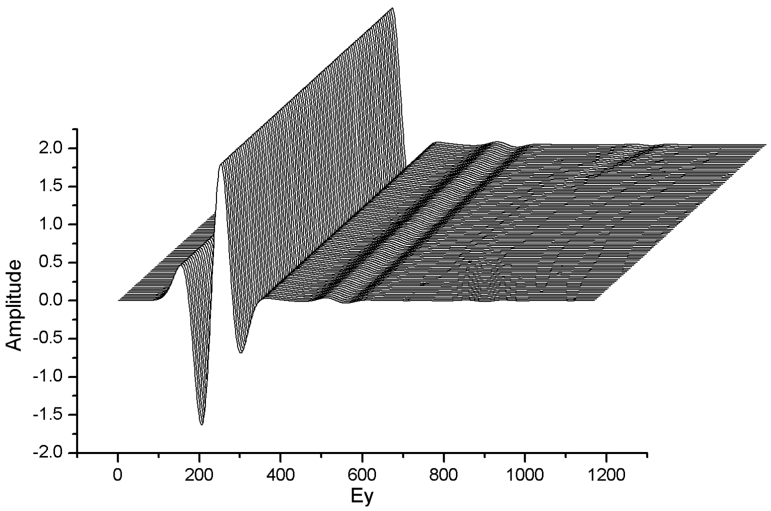

Figure 5:Ey component waveform profile of 97 channels of single-shot and single-receive radar

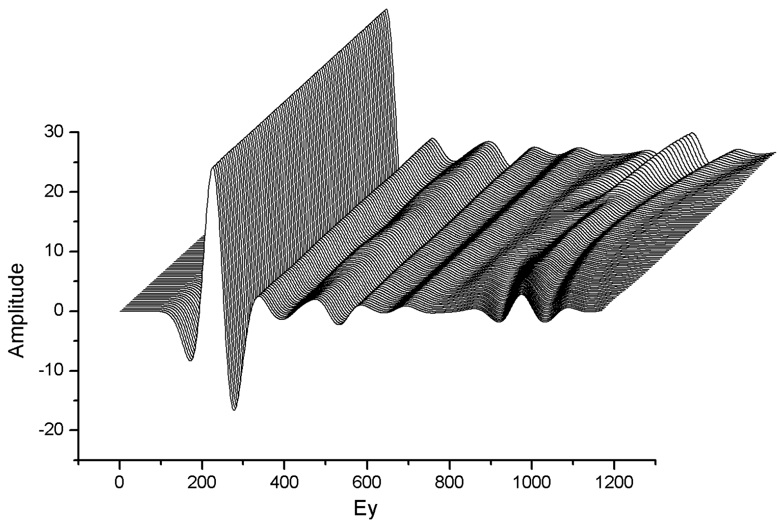

Figure 6:Ey component waveform profile of 97 channels of 8×8 array radar

Slice the array radar data volume to analyze the propagation characteristics of the array radar electromagnetic wave in three-dimensional space. Figure 7 shows the vertical slice along the y axis of the electric field (E) amplitude at 45 ns.In order to determine the spatial position of the metal ball, the three-dimensional data volume of the array radar is sliced along the x-axis and y-axis, and the vertical slice diagram of the x- and y-axis at 45 ns is shown in Figure 8.From the figure, we can clearly know the spatial position of the metal ball and the wave field propagation characteristics of the electromagnetic wave of the array transmitting antenna when it encounters various strata and metal balls.The electromagnetic wave has obvious reflection phenomenon at the position of the metal ball, which forms the hyperbola echo signal.

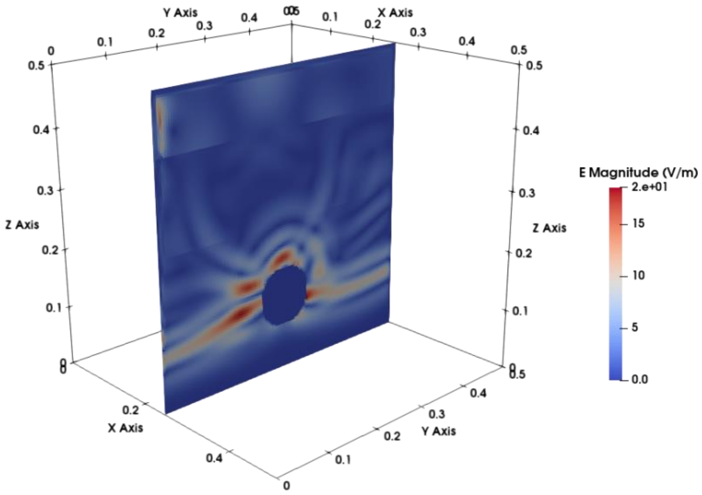

Figure 7: Vertical slice of the amplitude of 8×8 array radar electric field (E) along the y-axis at 45 ns

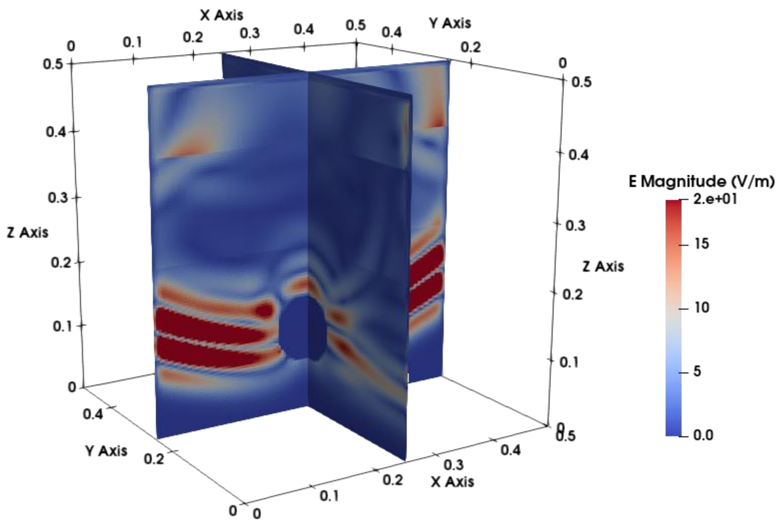

Figure 8 Vertical slice of the amplitude of 8×8 array radar electric field (E) along the x,y-axis at 45 ns

3.3 Comparative analysis of polarization characteristics:

The propagation of electromagnetic waves can be decomposed into a series of harmonics of different frequencies. The propagation of harmonics can be approximated as plane wave propagation.The excitation source uses Hertzian dipoles polarized in the z direction, and plane waves will undergo linear polarization,A plane wave propagating along the z-axis, the electric field (E) is parallel to the xy plane, and the electric field (E) can be decomposed into two components, Ex and Ey, which is:

$$E = a_x E_x + a_y E_y \qquad (33)$$

Where a_x, a_y are the direction vectors in the x and y directions respectively,E represents the sum of the vector field linearly polarized along the x direction and along the y direction.

Suppose the amplitude of E_x is E_{x0}, the amplitude of E_y is E_{y0}, and the lag phase is φ, and equation (33) is expressed as:

$$E(z) = a_x E_{x0} e^{-jkz} + a_y E_{y0} e^{-jkz} e^{-j\varphi} \qquad (34)$$

According to equation (34), the transient expression of the electric field at time t in the z-plane is obtained:

$$\begin{aligned} E(z,t) &= \mathrm{Re}\{[a_x E_{x0} + a_y E_{y0} e^{-j\varphi}] e^{-jkz} e^{-j\omega t}\} \\ &= a_x E_{x0} \cos(\omega t - kz) + a_y E_{y0} \cos(\omega t - kz - \varphi) \qquad (35) \end{aligned}$$

Where k is the wave number, ω is the angular frequency, and j is the complex unit.From equation (35), it can be seen that the polarization of the electric field at any time t in the z-plane is related to the amplitude value.At time=45ns,z=0.35m, z=0.125m,take the plane wave field,At this time, the electric field plane wave polarization of the array observation method is shown in Figure 9.Since the amplitude of the 8×8 array radar is approximately 10 times that of the single-shot single-receive radar, according to formula (35), when the amplitude of the electric field increases, the electric field component along the x, y direction on the z-plane at any time t The amplitude will be increased accordingly, and the polarization characteristics will be more obvious.It can be seen in Figure 9 that the array observation method has a very good polarization effect in the xy plane. Obvious polarization in the x and y directions occurs at the position of the metal ball in the x and y plane. The electric field is a plane wave in the Spread in the x, y plane, the size and shape of the target can be judged according to the polarization component.Single-shot and single-receive conventional common-offset observation method. The plane wave spreads in the form of a circle from a center point on the x and y planes. As shown in Figure 10, there is no obvious directional polarization in the metal sphere plane phenomenon.

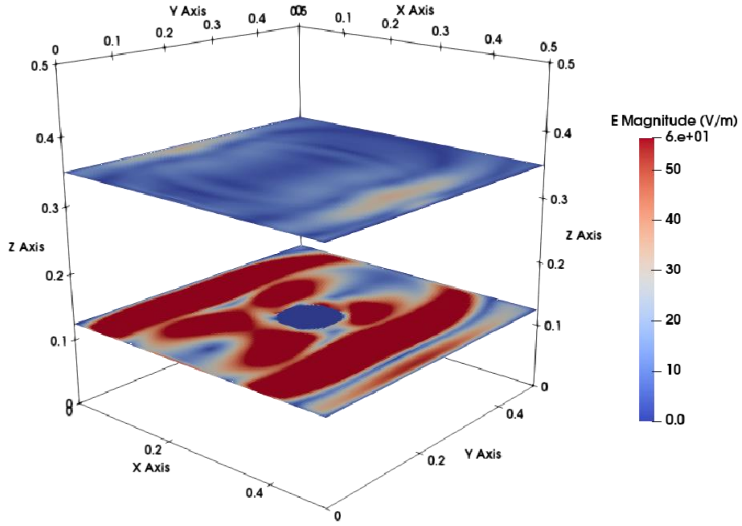

Figure.9 Polarization characteristic field of 8×8 array radar at 45ns

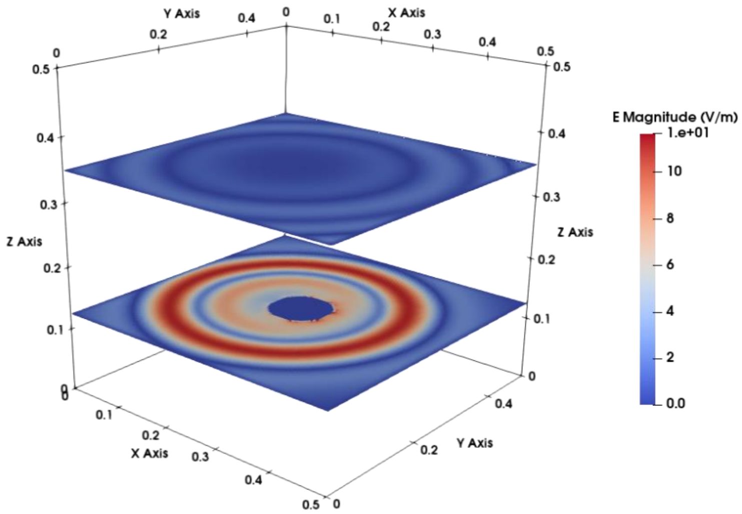

Figure.10 Polarization characteristic field of single-shot and single-receive radar at 45ns

Tracking the full waveform of array radar and single-shot single-receiving radar in three-dimensional space (which is Ex, Ey, Ez, Hx, Hy, Hz six wavefields), in the conventional single-input single-output common offset observation mode, the target echo signal propagates back to the receiving antenna along the incident path of the transmitted signal, and the electromagnetic wave spreads downward in the form of a spherical surface, therefore, the time-distance curve of the received signal is hyperbolic.In an 8×8 array radar, each transmitting antenna generates approximately the same signal, and the transmitting and receiving antennas radiate and receive in an isotropic or half-space isotropic medium. The transmit beam synthesized by the transmit signal array is approximately a plane wave signal, as shown in Figure 11-1.

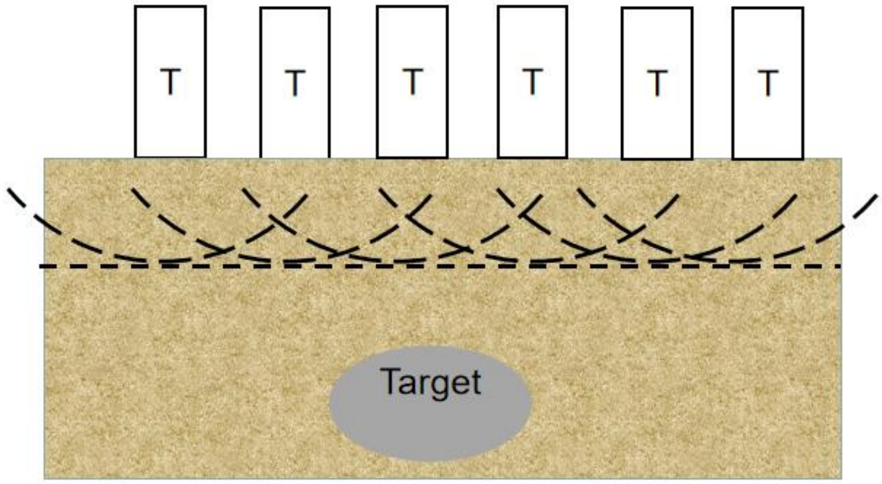

Figure 11-1 Schematic diagram of array radar wavefield reconstruction

Separate the electric field components of the conventional single-shot single-receiving radar and the 8×8 array radar, and obtain the three electric field components of the single-shot single-receiving radar as shown in Figure 11 (a, c, e).The x, y, and z components of the electric field all have obvious reflected echo signals when they encounter the metal ball. the x component of the electric field contributes a strong echo energy, and the reflected echo in the y, z direction is not Obviously, the downward propagation energy of the electric field component in the y direction is very strong.The schematic diagram of the three-component electromagnetic wave field propagation of the electric field of the 8×8 array radar is shown in Figure 11 (b, d, f). It can be clearly observed that the electromagnetic wave forms a plane beam during the downward propagation process, compared to The single-shot and single-receive radar excitation method, the three-component reflected echo signal of the electric field is obvious, and the contributions to the reflected echo signal energy in the three directions of x, y, and z are basically the same.This is because multiple transmitting antennas emit at the same time to form a uniform coverage of multiple points, and multiple receiving antennas receive at the same time, forming multiple angles to illuminate the target body. On the same plane, the electromagnetic energy is better scattered, and the receiving antenna can receive To reflect information from different angles of the target.

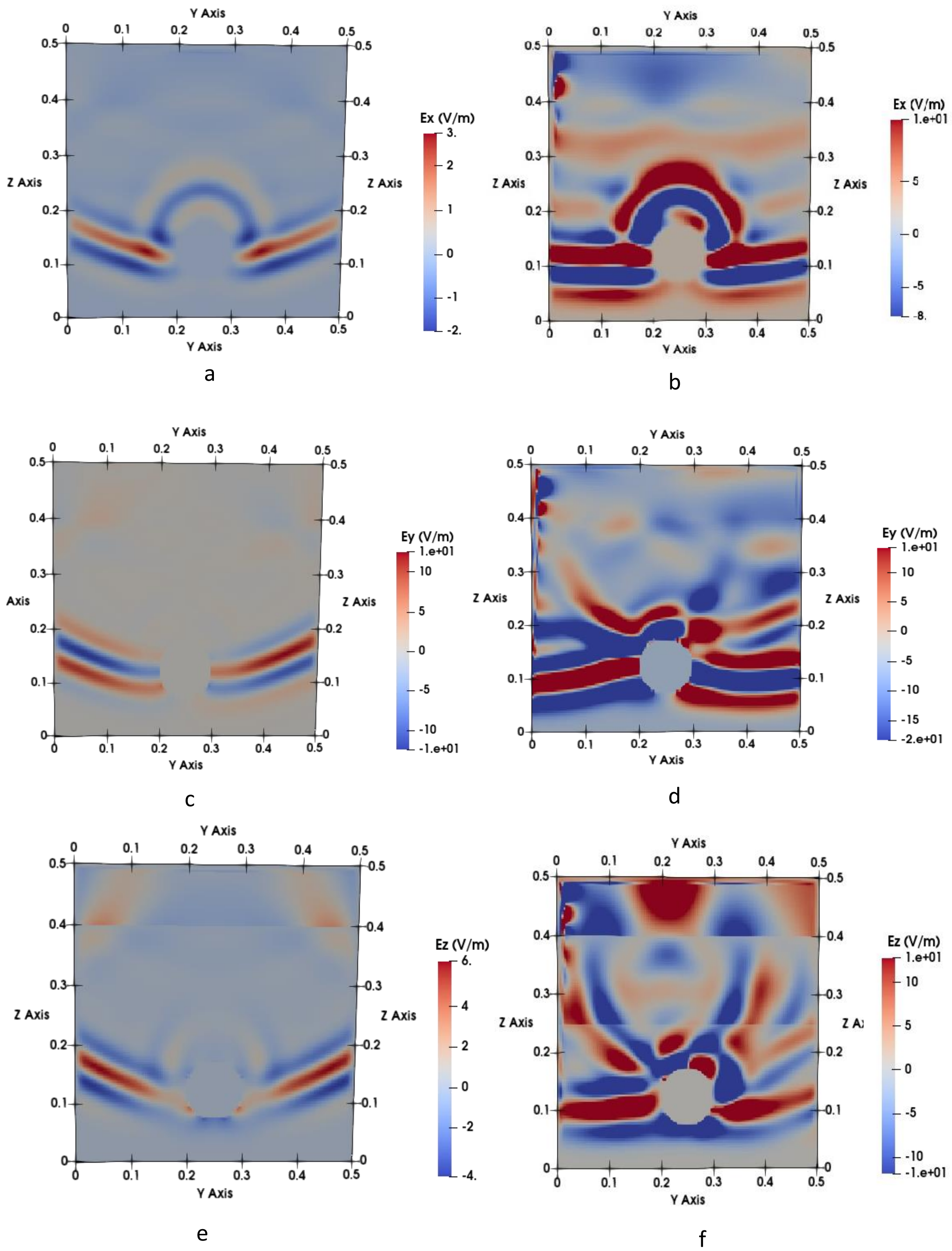

Figure 11 Recording diagram of each component of TE wave of single-shot single-receive radar

and array radar at 45ns

a Single-shot and single-receive Ex component wave field

b 8×8 array radar Ex component wave field

c Single-shot and single-receive Ey component wave field

d 8×8 array radar Ey component wave field

e Single-shot and single-receive Ez component wave field

f 8×8 array radar Ez component wave field

Separate the magnetic field along the x, y, z directions in the three-dimensional space to obtain the three components of the single-shot single-receiving radar magnetic field, as shown in Figure 12 (h, j, m). It can be observed that the single-shot single-receive magnetic field is also spherical The form of propagating downwards, on the x component of the magnetic field, the reflected magnetic component is very weak, almost approaching zero, and the y component of the magnetic field has a more obvious reflected echo signal.Because the Hertzian dipole polarized along the z direction is used as the excitation source, the z direction of the magnetic field forms a magnetic field signal as shown in Figure 12 (m).This is because electromagnetic waves consist of electric and magnetic fields that are perpendicular to each other. When the electromagnetic wave is polarized along the z-direction, it encounters a metal body, the electric field will be inside the metal body (conducting), the magnetic field forms a left and right-hand polarization phenomenon, spreading around the metal ball.In the same way, separate the three-component diagram of the magnetic field of the 8×8 array radar, and obtain the three-component diagram of the magnetic field as shown in Figure 12 (i, k, n). It can be clearly observed that the magnetic field also forms a plane beam and propagates downward. At this time, the echo signal reflected by the target body can be observed in three directions of the magnetic field.Especially for the electromagnetic wave around the small metal sphere, the wave field is clearer, and the reflected echo signal is more obvious.

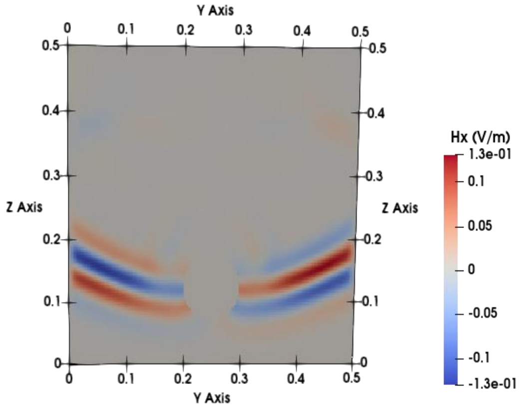

h

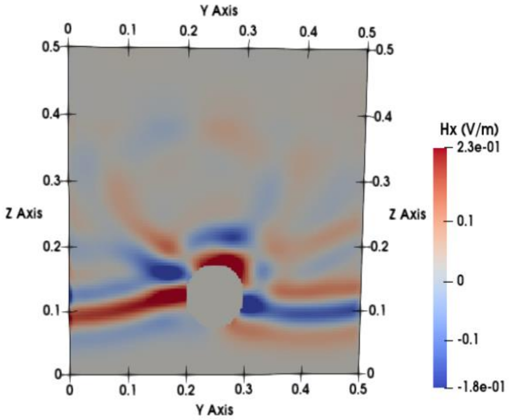

i

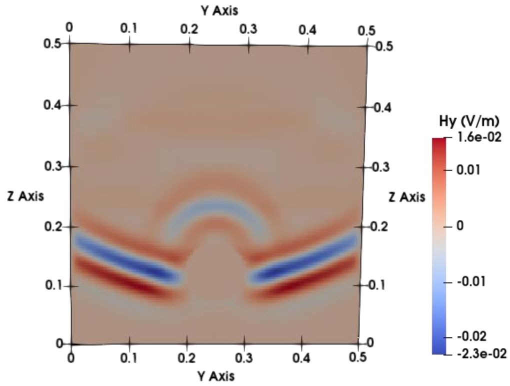

j

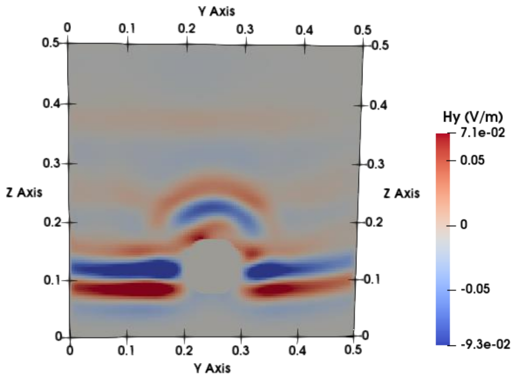

k

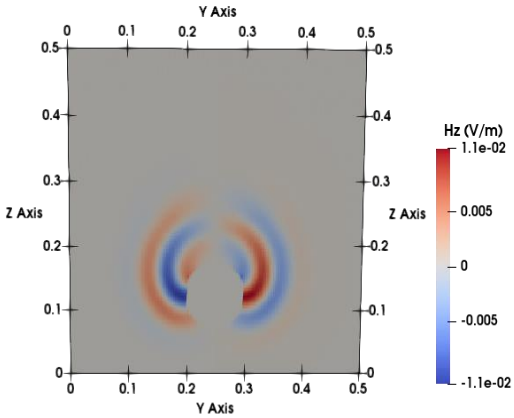

m

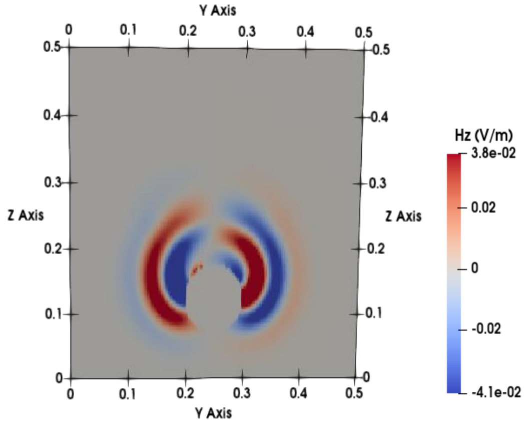

n

Figure 12 Recording diagram of each component of TM wave of single-shot single-receive radar and array radar at 45ns

h Single-shot and single-receive Hx component wave field i 8×8 array radar Hx component wave field

j Single-shot and single-receive Hy component wave field

k 8×8 array radar Hy component wave field

m Single-shot and single-receive Hz component wave field

n 8×8 array radar Hz component wave field

Planar electromagnetic waves can always be decomposed into two orthogonal linearly polarized waves. When a linearly polarized electromagnetic wave is emitted, the target has a depolarization effect after being scattered by a natural target, so there is not only the same effect in the echo signal. The polarization component should also have a cross-polarization component. When the polarization state of the receiving antenna and the echo are the same, the received echo energy reaches the maximum value, and the array radar will have a full polarization effect in space, so it can be better To capture the morphological characteristics of the target to enhance the echo energy.Comparing the full waveforms of the electric field and magnetic field components of the array radar and the single-shot single-receiving radar in Fig. 11 and Fig. 12, it is found that the array observation method can obtain relatively high signal stability in the direction of each component of the electric field and the magnetic field compared with the conventional observation method. The target signal has higher energy and better quality. The plane wave signal formed by the array observation method covers all points of the target body, and the scattering signal of the target body is better. After one scan, the size of the target body can be judged and a clearer reflection signal can be obtained.

4 Conclusion

1. Array radar has a wide range of scanning at one time when detecting the target body, which can greatly improve the detection efficiency. The observation method of multiple transmitting antennas simultaneously stimulating electromagnetic waves increases the energy of echo signal greatly due to the overlapping of energy. Compare the detection mode of single dispatch and single reception radar, can achieve the same goal with better lighting. Make Sectional figure and Slice figure of the 3d array radar data at different positions, is a good way to explain a reflection of electromagnetic waves in different media effect, launch more receive more observation method,

on the space to expand the detection efficiency. One scan can get the wave field propagation characteristics of a wider underground medium.Feedback more comprehensive underground formation structure information.

2. Use the complex frequency shift perfectly matched layer (CFS-PML) as the absorbing boundary condition to effectively absorb electromagnetic waves at the boundary. This method is not affected by the angle of incidence, It has a better electromagnetic wave absorption effect than the traditional PML method.

3.Multi-transmitting and multi-receiving array radar observation method can combine any transmitting antenna and receiving antenna, Each receiving antenna receives superimposed electromagnetic waves from different transmitting antennas, The combination of transmitting antenna and receiving antenna can be diversified, It is expected to scan the target body in three dimensions.

4.Polarization can well describe the position and shape of the target body, Electromagnetic waves can be better polarized under the array observation mode, also contains rich target body information，Get more ideal detection data.However, due to the phase of multi-transmitting and multi-receiving array ground penetrating radar, electromagnetic waves will interfere with different degrees,therefore, The analysis and phase correction of the polarization characteristics of the array ground penetrating radar in different media and different target shapes will be the next research target.

Acknowledgments and data:

The Model file is stored in the Model File directory(https://doi.org/10.4121/12936149;Last access: September 2020) of 4 tu.ResearchData database(https://data.4tu.nl/account/home). The Model output file calculated based on the Model is stored in the Kongdong_merged.Out directory(https://doi.org/10.4121/12935972;Last access :September 2020) of 4 Tu.ResearchData database(https://data.4tu.nl/account/home). The calculated 60 nanossecond wave field data and wave field propagation animation are stored in the Array radar wave field animation(https://doi.org/10.4121/12936803,Last access: September 2020) of 4 tu.ResearchData database(https://data.4tu.nl/account/home).The package, located under the Paraview file directory(https://doi.org/10.4121/12936899,Last access: September 2020) of four tu.ResearchData databases(https://data.4tu.nl/account/home), uses version 5.8 of the software, available on its official website at (https://www.paraview.org/). And special thanks to the editor for allowing the deadline extension during the COVID-19 pandemic.

5. References

[1] Li Hua, LU Guangyin, HE Xianqi, Deng Ke.Development history and prospect of ground penetrating radar [J]. Progress in geophysics,2010,25(04):1492-1502. https://doi.org/CNKI:SUN:MDKT.0.1997-05-019.

[2] T. Jin, J. Lou and Z. Zhou, "Extraction of Landmine Features Using a Forward-Looking Ground-Penetrating Radar With MIMO Array," in IEEE Transactions on Geoscience and Remote Sensing, vol. 50, no. 10, pp. 4135-4144, Oct. 2012. https://doi.org/doi: 10.1109/TGRS.2012.2188803.

[3] Si-Xin L , Yan-Qian F , Lei F U , et al. Advances and numerical simulation of airborne ground penetrating radar[J]. Progress in Geophysics, 2012, 27(2):727-735.https://doi.org/10.6038/j.issn.1004-2903.2012.02.040.

[4] Chai M , Xiao T , Zhao G , et al. A Hybrid PSTD/ADI-CFDTD Method for Mixed-Scale Electromagnetic Problems[J]. IEEE Transactions on Antennas & Propagation, 2007, 55(5):p.1398-140.https://doi.org/10.1109/TAP.2007.895630.

[5] X .Zeng,G.A.McMechan, J .Cai ,and H .W .Chen,“ Comparison of ray and Fourier methods for modeling monostatic ground penetrating radar profiles, ” Geophysics, vol60, no. 6, p p . 1727 –1734, 1995.https://doi.org/10.1190/1.1443905.

[6] Huang Y，Zhang J，Liu Q H.2011.Three-dimensional GPR ray tracing based on wavefront expansion with irregular cells［J］. IEEE Transactions on Geoscience and Remote Sensing，49(2) : 679-687. https://doi.org/10.1109/TGRS.2010.2061856.

[7] K. S. Yee, "Numerical solution of initial boundary value problems involving Maxwell's equations in isotropic media," IEEE Trans. Antennas Propagat., vol. 14, no. 4, pp. 3

02-307,1966.https://doi.org/10.1109/TAP.1966.1138693.

[8] D.-S. Feng and Q.-W . Dai, "GPR numerical simulation of full wave field based on UPML boundary condition of ADI-FDTD, "NDT & E International, vol.44,no.6, pp.495–504,2011.https://doi.org/10.1016/j.ndteint.2011.05.001.

[9] An, Q (An, Qiang); Hoorfar,etc.Range Coherence Factor for Down Range Sidelobes Suppression in Radar Imaging Through Multilayered Dielectric Media[J].IEEE ACCESS vol.7, no. 9,pp. 66910-66918.https://doi.org/10.1109/ACCESS.2019.2911693.

[10] Xu Shi-che, LIU Bin. Forward magnetoelectromagnetic modeling of horizontal layer with continuous variation of conductivity stratification [J].Journal of Geophysics,1995(02):262-268.https://doi.org/10.1088/0256-307X/12/7/010.

[11] Howlader M O F , Sattar T P . FDTD based numerical framework for ground penetrating radar simulation[J]. Progress in Electromagnetics Research M, 2015, 44:127-138. https://doi.org/10.2528/PIERM15090304.

[12] Q. H. Liu, "The pseudospectral time-domain (PSTD) method: a new algorithm for solutions of Maxwell's equations," IEEE Antennas and Propagation Society International Symposium 1997. Digest, Montreal, Quebec, Canada, 1997, pp. 122-125 vol.1, doi: 10.1109/APS.1997.630102.https://doi.org/10.1109/APS.1997.630102.

[13] J. M. Carcione, S. Valle, and G. Lenzi, "GPR modelling by the Fourier method: improvement of the algorithm, " Geophysical Prospecting, vol.47,no.6, pp.1015–1029 , 1999.https://doi.org/10.1046/j.1365-2478.1999.00151.x.

[14] K. S. Yee, "Numerical solution of initial boundary value problems involving Maxwell's equations in isotropic media," IEEE Trans. Antennas Propagat., vol. 14, no. 4, pp. 302-307, 1966.https://doi.org/10.1109/TAP.1966.1138693.

[15] Oden C P , Wright D L , Powers M H , et al. Ground penetrating radar antenna system analysis for prediction of earth material properties[C]// Antennas & Propagation Society International Symposium. IEEE, 2005.https://doi.org/10.1109/APS.2005.1552436.

[16] Bai Z , Ma X , Zhuansun X , et al. An efficient application of PML in fourth-

order precise integration time domain method for the numerical solution of Maxwell's equations[J]. Compel International Journal for Computation & Mathematics in Electrical & Electronic Engineering, 2014, 33(1-2):págs. 116-125.https://doi.org/10.1108/COMPEL-10-2012-0272.

[17] Shangguan S , Qiu X , Yang J , et al. Extraction and Analysis of the Scattering Stability in Urban Areas Based on Dual-Polarization SAR Data[J]. IEEE Geoscience and Remote Sensing Letters, 2018.https://doi.org/10.1109/LGRS.2018.2873624.

[18] J R Huynen. Phenomenological theory of radar targets[D]. Netherlands: Technical University Delft, 1970.https://doi.org/doi:http://dx.doi.org/.

[19] Dino Giuli. Polarization diversity in radars[J]. Proceedings of IEEE, 1986, 74(2): 245-269.https://doi.org/10.1109/PROC.1986.13457.

[20] J. Xi, Z. Zeng, L. Huang,etc. Characteristics of the Signal Polarization Field in Array Type Ground Penetrating Radar[J]. Journal of Jilin University, 2017, 47(2):633-644..https://doi.org/10.13278/j.cnki.jjuese.201702307.

[21] Song P , Zhang Z , Liang L , et al. Study on Optimization of Parallel Efficiency of CPU-GPU Heterogeneous Parallelization for MOC Neutron Transport Calculation[J]. Yuanzineng Kexue Jishu/Atomic Energy ence and Technology, 2019, 53(11):2209-2217.https://doi.org/10.7538/yzk.2019.youxian.0416.

[22] Wang S , Wang C , Cai Y , et al. A novel parallel finite element procedure for nonlinear dynamic problems using GPU and mixed-precision algorithm[J]. Engineering Computations, 2020, ahead-of-print(ahead-of-print).https://doi.org/10.1108/EC-07-2019-0328.

[23] Wu Enhua, Liu Zhiquan. General Computing based on GPU [J].Journal of Computer-Aided Design and Graphics, 2004, 16(5):601-612.https://doi.org/10.3321/j.issn:1003-9775.2004.05.002.